Polar steric interactions for V-shaped molecules

Fulvio Bisi, Riccardo Rosso, and Epifanio G. Virga
Dipartimento di Matematica and CNISM, Università di Pavia, Via Ferrata 1, 27100 Pavia, Italy

Georges E. Durand
Laboratoire de Physique des Solides associé au CNRS (LA2), Université Paris Sud, F-91405 Orsay Cedex, France
(Received 14 December 2007; revised manuscript received 1 April 2008; published 17 July 2008)

We consider the effect of shape polarity in the excluded-volume interaction between V-shaped polar particles in orientationally ordered phases. We show that the polar component of the steric interaction between these polar particles, large enough in two space dimensions, can also become important in three space dimensions. Unexpectedly, polar steric interactions, up to now neglected, favor an "antiparallel" pair binding, which may be the building block of orientationally ordered phases for polar particles. An *antiferromorphic* smectic ordering, which is also antiferroelectric, could further be attained at high enough density by the same mechanism.

DOI: 10.1103/PhysRevE.78.011705 PACS number(s): 61.30.Cz, 61.30.Gd

I. INTRODUCTION

For a long time, hard-core particles have been used to model phase transitions in ordered fluids [1]. In these models, two hard particles with shapes Ω and Ω' and volumes V and V' tend to occupy the largest accessible volume, to maximize their entropy. For a given relative orientation of these particles, the *excluded region* Ω^* is not accessible to any point of one particle when its boundary glides without rolling on the boundary of the other particle; the volume of Ω^* is the *excluded volume* $V^*(\Omega,\Omega')$, which depends on both shapes Ω and Ω'. Maximizing the volume available to Ω and Ω' amounts to minimize their mutually excluded volume. Increasing the particle density may result in an orientational ordering transition, which may be followed by a positional ordering transition. Much work has been devoted to this problem for central-symmetric shapes in liquid crystals and, more recently, nanoparticles [2]. Recent interest in biaxial liquid crystals focused attention on V-shaped molecules [3–7]. Because this shape is not central symmetric, possible polar effects on V^* need be considered; they cannot always be regarded as negligible, as they were in [8]. This comment applies in general to all non-central-symmetric shapes. We shall show in Sec. II that in two space dimensions the excluded area of V-shaped rods exhibits a large polarity: the difference between the excluded area in the parallel, "$\langle\langle$," and antiparallel, "$\langle\,\rangle$," configurations is appreciable. The question is then whether such a polar effect persists in three space dimensions for excluded volumes. In Sec. III, we answer this question for V-shaped particles in a class of C_{2v}-symmetric shapes. In Sec. IV, we extend our conclusions to $C_{\infty v}$-symmetric shapes and envisage possible physical applications of the polar interaction described in this paper.

II. POLARITY INDEX IN THE PLANE

In this section, our primary objective is describing shape polarity in purely steric interactions and devising an appropriate measure for it. We begin by considering the simple example illustrated in Fig. 1.

In Fig. 1(a), two equal V-shaped rods in the plane $\mathcal{S}$ are in the parallel configuration, with the two apexes in contact: one V is black, while the other is white; both have equal arms. While the white V glides over the black V, a region remains inaccessible to the apex of the former by the presence of the latter, which appears shaded in Fig. 1(a); it has area $A^*_{\langle\langle}$. Similarly, as illustrated in Fig. 1(b), when the black and white V's are in the antiparallel configuration, gliding the white V over the black V produces the shaded excluded region with area $A^*_{\langle\,\rangle}$. Simple geometric considerations show that

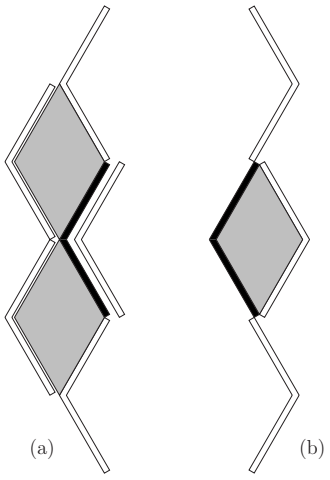

FIG. 1. Two interacting V-shaped particles, Ω and Ω', are depicted as black and white, respectively. (a) Parallel configuration. The shaded region is inaccessible to the apex of Ω' when this glides over Ω. The excluded area starts building up when the ends of the two particles come in contact. (b) Antiparallel configuration. The shaded region is inaccessible to the apex of Ω' when this glides over Ω. The excluded area starts building up when the end of one particle comes in contact with the apex of the other. The excluded area in (a) is twice as large as in (b), and so, according to the definition (3), $I_p=1$ in (a) and $I_p=-1$ in (b).

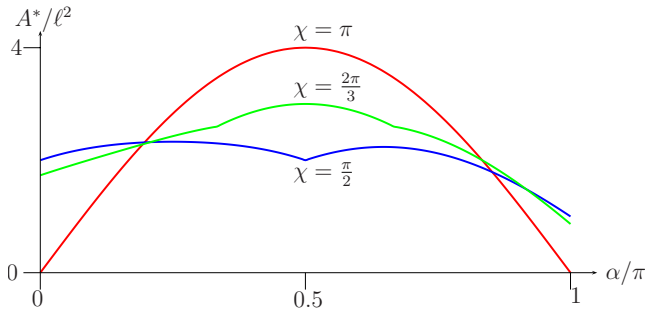

FIG. 2. (Color online) Plots of the excluded area A^* of two V-shaped rods against the rotation angle $\alpha\in[0,\pi]$, for $\chi=\frac{\pi}{2}$ (blue), $\chi=\frac{2\pi}{3}$ (green), and $\chi=\pi$ (red). The analytic expression for A^* is computed in the Appendix ; for $\chi=\pi$ it coincides with the excluded area of two straight rods with length 2ℓ.

$$A^*_{\langle\,\rangle}=\frac{1}{2}A^*_{\langle\langle}. \tag{1}$$

Thus, the parallel configuration cannot possibly minimize the excluded area of the two rods; symmetry suggests that their excluded area is minimized by the antiparallel configuration. To prove this properly, we need compute the excluded area A^* of the two rods as a function of the angle α of their relative rotation.

The function $\alpha\mapsto A^*(\alpha)$ enjoys a symmetry property that eases its computation. Exchanging α with $2\pi-\alpha$ amounts to exchanging the role of the two shapes; since these are identical, exchanging them does not affect their excluded area, and so

$$A^*(\alpha)=A^*(2\pi-\alpha). \tag{2}$$

In particular, this illustrates that it suffices to know A^* in the interval $[0,\pi]$ to determine it in the whole interval $[0,2\pi]$.

Let ℓ be the length of each arm in a single rod and let $\chi\in[0,\pi]$ be the inter-arm angle. For definiteness, we shall assume that $\chi\geqslant\frac{\pi}{2}$, though our development can easily be adapted to the case where $0\leqslant\chi\leqslant\frac{\pi}{2}$. In the Appendix we present all the computational details needed to determine analytically the function $\alpha\mapsto A^*(\alpha)$. A^* is plotted in Fig. 2 against $\alpha\in[0,\pi]$ for $\chi=\frac{\pi}{2}$ and $\chi=\frac{2\pi}{3}$ in units ℓ^2; both graphs are contrasted against the plot obtained in the limit as $\chi\to\pi$, corresponding to the excluded area $A^*_{\chi=\pi}=4\ell^2\sin\alpha$ of two straight rods with length 2ℓ.

As expected, for all values of χ, A^* attains its minimum at $\alpha=\pi$. Moreover, for χ sufficiently larger than $\frac{\pi}{2}$, A^* attains no local minimum in the interior of the interval $[0,\pi]$.

To illustrate better the polarity exhibited by the function A^*, we found it useful to introduce the *polarity index* I_p, defined as

$$I_p(\alpha):=3\frac{A^*(\alpha)-A^*(\alpha+\pi)}{A^*(\alpha)+A^*(\alpha+\pi)}, \tag{3}$$

for $\alpha\in[0,2\pi]$. For $\alpha=0$, I_p clearly compares the difference in excluded area between the parallel and antiparallel configurations of the shapes Ω and Ω' to the sum of their excluded areas, the numerical factor being chosen so as to make $I_p(0)=1$. More generally, for $\alpha>0$, I_p similarly estimates the difference between the excluded area between the shapes Ω and Ω' in the configuration where Ω' is rotated by the angle α with respect to Ω, and the configuration where the rotated Ω' is inverted relative to its apex. To illuminate this interpretation of I_p, we recall that in a plane $\mathcal{S}$ all rotations $\mathbf{R}_\perp$ about a unit vector $\boldsymbol{e}$ orthogonal to $\mathcal{S}$ can be represented as

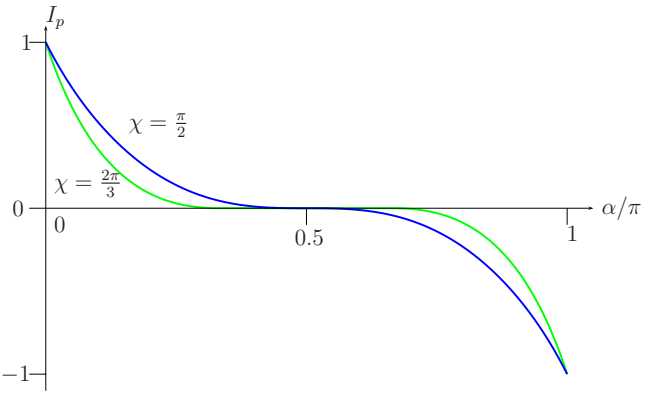

FIG. 3. (Color online) Plots of the polarity index I_p as defined in Eq. (5), for $\chi=\frac{\pi}{2}$ (blue) and $\chi=\frac{2\pi}{3}$ (green).

$$\mathbf{R}_\perp(\alpha)=\sin\alpha\mathbf{W}+\cos\alpha\mathbf{P}, \tag{4}$$

where $\mathbf{W}$ is the skew symmetric tensor associated with $\boldsymbol{e}$ and $\mathbf{P}$ is the projection onto $\mathcal{S}$. It follows immediately from (4) that

$$-\mathbf{R}_\perp(\alpha)=\mathbf{R}_\perp(\alpha+\pi),$$

showing formally that a central inversion on $\mathcal{S}$ amounts to a rotation by π about the unit vector $\boldsymbol{e}$ through the center of inversion. On the other hand, by (2),

$$A^*(\alpha+\pi)=A^*(\pi-\alpha),$$

so that Eq. (3) becomes

$$I_p(\alpha)=3\frac{A^*(\alpha)-A^*(\pi-\alpha)}{A^*(\alpha)+A^*(\pi-\alpha)}. \tag{5}$$

It should finally be observed that it follows from (3) and (5) that

$$I_p(\alpha+\pi)=-I_p(\alpha) \tag{6}$$

and

$$I_p\left(\alpha+\frac{\pi}{2}\right)=-I_p\left(\frac{\pi}{2}-\alpha\right), \tag{7}$$

respectively, and so it suffices to determine I_p in $[0,\frac{\pi}{2}]$, to know it in the whole of $[0,2\pi]$. In particular, by (7), $I_p(\frac{\pi}{2})=0$. Figure 3 shows the plots of I_p in $[0,\pi]$ for both $\chi=\frac{\pi}{2}$ and $\chi=\frac{2\pi}{3}$.

These graph, which are smoother than the corresponding graphs for A^*, give a clear indication of how polar the steric interaction of V-shaped particles is: the higher the degree of polarity, the wider the range where I_p is different from zero. In the limit $\chi\to\pi$, this steric interaction fails to be polar as

TABLE I. Odd cosine Fourier coefficients for the function $I_p(\alpha)$ defined as in Eq. (8).

χ	a_1	a_3	a_5	a_7
$\frac{\pi}{2}$	0.47	0.24	0.088	0.048
$\frac{2\pi}{3}$	0.33	0.24	0.13	0.067

the rods become straight; correspondingly, I_p tends to zero in the whole of $[0,\pi]$, but not uniformly, as $I_p(0)=1$ and $I_p(\pi)=-1$ for every $\chi<\pi$.

Another way to measure the degree of polarity represented by I_p is computing its cosine Fourier coefficients,

$$a_k := \frac{1}{\pi}\int_0^{2\pi} I_p(\alpha)\cos(k\alpha)\mathrm{d}\alpha = \frac{2}{\pi}\int_0^{\pi} I_p(\alpha)\cos(k\alpha)\mathrm{d}\alpha, \tag{8}$$

for $k\in\mathbb{N}$, being all sine Fourier coefficients of I_p zero, by (6). Moreover, by (7), all even-indexed coefficients a_k vanish. In particular, we call a_1 and a_3 the *dipolar* and *octupolar* coefficients. Table I reproduces the nonvanishing coefficients a_1 through a_7 for $\chi=\frac{\pi}{2}$ and $\chi=\frac{2\pi}{3}$.

They clearly indicate that the dipolar and octupolar components of I_p prevail over the others and that the former indeed embodies most qualitative features of the polar steric effect we describe here. A similar behavior is exhibited by the excluded area A^* itself. Its cosine Fourier coefficients, which by (2) can be written as

$$A_k := \frac{2}{\pi}\int_0^{\pi} A^*(\alpha)\cos(k\alpha)\mathrm{d}\alpha, \tag{9}$$

are reported in Table II for $1\leqslant k\leqslant 7$.

The alternating sign in the A_k sequence shows an antagonism between even-indexed and odd-indexed harmonics, which again reveals the polarity of the purely steric interaction between V-shaped rods. While the *quadrupolar* component $(k=2)$ of this interaction, like all other even-indexed harmonics, would equally promote either the parallel and the antiparallel configurations as a minimizer of the excluded area, the dipolar component $(k=1)$, like all other odd-indexed harmonics, would prefer the antiparallel configuration. Moreover, Table II suggests that for sufficiently wide V's the dipolar, quadrupolar, and octupolar components of the steric interaction could suffice to describe it rather faithfully, whereas higher even-indexed harmonics might be needed for narrower V's.

TABLE II. Cosine Fourier coefficients for the function $A^*(\alpha)$ defined as in Eq. (9). Here the coefficient A_0, though different from zero, is not reported as it corresponds to the isotropic component of A^*.

χ	A_1	A_2	A_3	A_4	A_5	A_6	A_7
$\frac{\pi}{2}$	0.29	−0.21	0.13	−0.19	0.030	−0.018	0.014
$\frac{2\pi}{3}$	0.18	−0.69	0.12	−0.088	0.052	−0.097	0.019

The simple geometric construction that leads one to establish Eq. (1) can be extended to establish the same conclusion for all pairs of equal V-shaped curves, not necessarily enjoying the C_{2v} symmetry. In particular, Eq. (1) will be proved in [9] for the excluded area of any pair of equal planar arcs along which the curvature does not vanish and the total angular variation of the oriented tangent does not exceed π. This shows that I_p, as given by (5), ranges in the interval $[-1,1]$ for all such general V-shaped curves.

The above quantitative details support the idea that the polarity index I_p effectively describes the role of shape polarity in steric interactions. A criticism could, however, be made on this definition: its validity seems to be limited to the two-dimensional realm. More severely, the polarity of steric interactions described by I_p could abruptly fade away as the shapes Ω and Ω' leave their common symmetry plane $\mathcal{S}$. The simple example worked out here cannot answer this question, as it is intrinsically two-dimensional. In the following section, with the aid of a truly three-dimensional model for V-shaped particles, we shall compute an appropriately extended polarity index.

III. POLARITY INDEX OUT OF THE PLANE

We consider here the general class $\mathcal{C}$ of three-dimensional C_{2v}-symmetric shapes. For a shape $\Omega\in\mathcal{C}$ we call $\mathcal{S}$ the symmetry plane on which the shape is most extended and $\mathcal{S}_\perp$ the symmetry plane orthogonal to it. Any polar quantity for $\Omega\in\mathcal{C}$ can be represented by a vector along the *polar axis* $\boldsymbol{p}$ common to $\mathcal{S}$ and $\mathcal{S}_\perp$. We denote by $\bar{\Omega}$ the central inverse of Ω. Here, as in Sec II, $\bar{\Omega}$ is obtained from Ω through a rotation by the angle π about the axis $\boldsymbol{e}$ orthogonal to $\mathcal{S}$ passing through the center of inversion: the polar axis of $\bar{\Omega}$ is thus $\bar{\boldsymbol{p}}=-\boldsymbol{p}$. To explore the effect of polarity on the excluded volume $V^*(\Omega,\Omega')$, we introduce the natural extension to this three-dimensional setting of the polarity index in Eq. (3) as

$$I_p(\Omega,\Omega') := 3\frac{V^*(\Omega,\Omega') - V^*(\Omega,\overline{\Omega'})}{V^*(\Omega,\Omega') + V^*(\Omega,\overline{\Omega'})}. \tag{10}$$

By symmetry, we expect I_p to attain its extrema when Ω and Ω' share the same symmetry planes.

Explicit excluded-volume computations are difficult [10]. A method has recently been established for particles represented as aggregates of (possibly overlapping) spheres [11]. In this class of shapes, Ω^* is itself an aggregate of spheres. We mimic a V-shaped particle by building from a central sphere two straight arms at an angle $\chi\in[\frac{\pi}{3},\pi]$, each with n adjacent spheres with equal radius (see Fig. 4).

We first examine the case where $n=1$. We start by computing V^* when Ω and Ω' are *coplanar*, that is, with their symmetry planes $\mathcal{S}$ and $\mathcal{S}'$ coincident; this is essentially a two-dimensional case, which parallels that already studied in Sec. II. Letting $\boldsymbol{p}\cdot\boldsymbol{p}'=\cos\alpha$, I_p is reduced to a function of α in the parameter χ. As expected, we find that $I_p=0$ for all χ, when $\boldsymbol{p}\cdot\boldsymbol{p}'=0$. Moreover, for all χ, I_p has the same polarity as $\boldsymbol{p}\cdot\boldsymbol{p}'$, though its spectral expansion is likely to contain all odd powers of $\boldsymbol{p}\cdot\boldsymbol{p}'$. For coplanar Ω and Ω', in Fig. 5 we show I_p as a function of α for $\chi=\frac{\pi}{2}$ and $\chi=\frac{2\pi}{3}$.

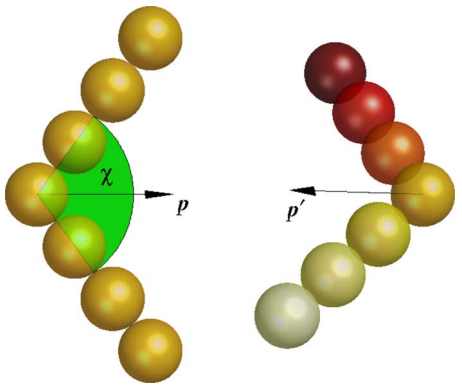

FIG. 4. (Color online) A three-dimensional rendering of two V-shaped particles Ω and Ω' constituted by $2n+1$ adjacent spheres with equal radius. Here $n=3$, χ is the interarm angle, $\boldsymbol{p}$ and $\boldsymbol{p}'$ denote the unit vectors along the polar axis of each shape. The closer the color of a sphere is to light yellow (light gray), the closer the sphere is to the observer's eye; the closer the color of a sphere is to dark red (dark gray), the farther the sphere is from the observer's eye.

These graphs should be compared with those in Fig. 3 for two-dimensional V-shaped rods. The variation of I_p in the whole interval $[0,\pi]$ is here smaller than in Fig. 3; typically, $I_p=0.15$ in Fig. 5. Moreover, for $\alpha=0$, I_p is greater for $\chi=\frac{\pi}{2}$ than for $\chi=\frac{2\pi}{3}$. For $n=1$, the first two nonvanishing cosine Fourier coefficients of I_p are $a_1=0.012$ and $a_1=0.082$ for $\chi=\frac{\pi}{2}$, and $a_1=0.030$ and $a_3=0.035$ for $\chi=\frac{2\pi}{3}$. Thus, the dipolar and octupolar contributions to the spectral decomposition of I_p are comparable for $\chi=\frac{2\pi}{3}$, while the octupolar contribution prevails for $\chi=\frac{\pi}{2}$.

Such a prevalence of the octupolar component, which has no analogue for two-dimensional V-shaped rods, is a consequence of the particle being stocky when n is small. To recover the slender arms of a V-shaped rod, n must be increased considerably. Tables III and IV present the first four nonvanishing cosine Fourier coefficients of I_p as a function of α for n ranging from 1 to 8 and interarm angle $\chi=\frac{\pi}{2}$ and $\chi=\frac{2\pi}{3}$, respectively.

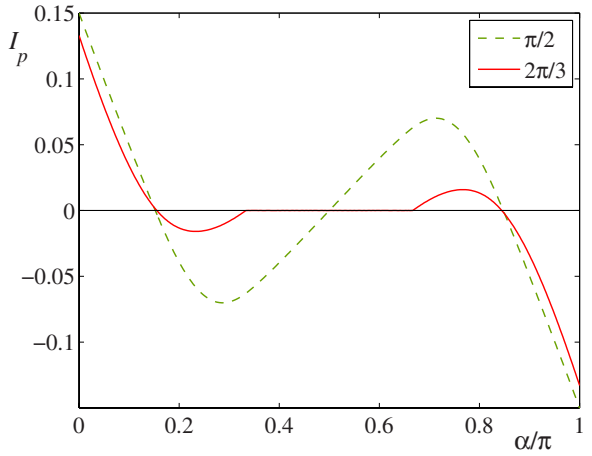

FIG. 5. (Color online) The polarity index I_p defined in Eq. (10) for Ω and Ω' as in Fig. 4 is plotted against the rotation angle α for $n=1$ and $\chi=\frac{\pi}{2}, \frac{2\pi}{3}$. I_p vanishes at $\alpha=\frac{\pi}{2}$, for all χ. While in the graph for $\chi=\frac{2\pi}{3}$ the dipolar component (proportional to $\cos\alpha$) is comparable to the octupolar component (proportional to $\cos 3\alpha$), in the graph for $\chi=\frac{\pi}{2}$ the octupolar component prevails over the dipolar component (see also Tables III and Table IV); both graphs display a distinct polar character.

TABLE III. First four nonvanishing cosine Fourier coefficients of the polarity index I_p for V-shaped particles like those depicted in Fig. 4 with n ranging from 1 to 8 and interarm angles $\chi=\frac{\pi}{2}$.

n	a_1	a_3	a_5	a_7
1	0.012	0.082	0.026	0.0051
2	0.081	0.11	0.031	0.015
3	0.14	0.13	0.036	0.020
4	0.18	0.14	0.041	0.023
5	0.21	0.15	0.045	0.025
6	0.24	0.16	0.048	0.027
7	0.26	0.17	0.051	0.029
8	0.28	0.17	0.054	0.030

It clearly emerges from them the way in which a_1 grows larger than a_3 as n increases, and how it overcomes a_3 earlier for $\chi=\frac{2\pi}{3}$ than for $\chi=\frac{\pi}{2}$. The upper limit $n=8$ is recommended by the present version of the numerical code employed here; on the other hand, for $n=8$ the major qualitative features of slender V-shaped particles are already sufficiently manifest.

Figure 6 illustrates the graphs of I_p for $\chi=\frac{\pi}{2}$ and n ranging from 1 to 8: they show how the variation of I_p in $[0,\pi]$ steadily increases with increasing n, making I_p resemble more the polarity index for a V-shaped rod in Fig. 3.

This asymptotic behavior is illuminated by computing I_p for $\alpha=0$ as a function of χ and n. We adopted an analytic recursive procedure explained in [11], which led us to the graphs for $I_p(\chi,n)$ plotted in Fig. 7. For $n=1$, I_p is small. On the other hand, for large n, I_p saturates to 1 whatever may be χ, except π.

To explore the three-dimensional dependence of I_p in Eq. (10), we now consider the case where Ω and Ω' are no longer coplanar. It follows from the C_{2v} symmetry that the two relevant geometric parameters describing the out-of-plane configurations of Ω and Ω' are the *bend* angle β and

TABLE IV. First four nonvanishing cosine Fourier coefficients of the polarity index I_p for V-shaped particles like those depicted in Fig. 4 with n ranging from 1 to 8 and interarm angle $\chi=\frac{2\pi}{3}$.

n	a_1	a_3	a_5	a_7
1	0.030	0.035	0.028	0.012
2	0.077	0.067	0.042	0.018
3	0.11	0.090	0.053	0.024
4	0.14	0.11	0.062	0.028
5	0.16	0.12	0.068	0.032
6	0.18	0.13	0.074	0.035
7	0.19	0.14	0.078	0.037
8	0.20	0.15	0.082	0.039

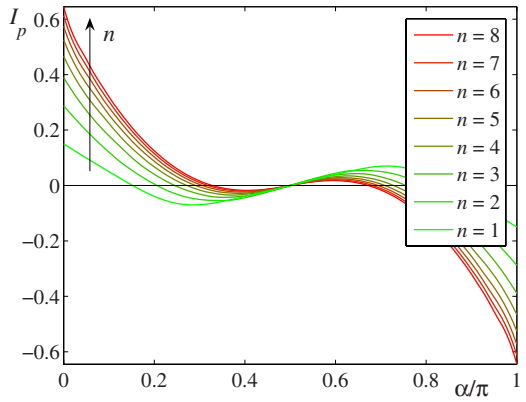

FIG. 6. (Color online) The graph of I_p against the angle $\alpha \in [0,\pi]$ for polar shapes Ω and Ω' like those in Fig. 4 with $\chi=\frac{\pi}{2}$ and $n=1,\ldots,8$, in the coplanar configuration. An arrow indicates the direction of increase of n through the plots.

the *twist* angle γ shown in Figs. 8 and 9.

For $\chi=\frac{\pi}{2}$, Figs. 10 and 11 illustrate I_p as a function of β and γ, respectively, when n ranges from 1 to 8. By contrasting Fig. 10 with Fig. 11, one easily sees how the decay of I_p with increasing n is more pronounced in the angle γ than in the angle β. We conjecture that the solid angle Δ within which I_p is appreciably different from zero decays like $\frac{1}{n^2}$ as n is increased. On the other hand, both Figs. 10 and 11 show that increasing n makes the variation of I_p larger. Combining these antagonistic tendencies, we easily anticipate that for large n the polarity of the steric interaction between V-shaped particles increases in strength, while becoming essentially two dimensional. By contrast, for small n, such a shape polarity, though weak, is truly three dimensional.

IV. DISCUSSION AND PERSPECTIVES

We have shown that V-shaped particles in the coplanar configuration exhibit the largest possible shape polarity, but

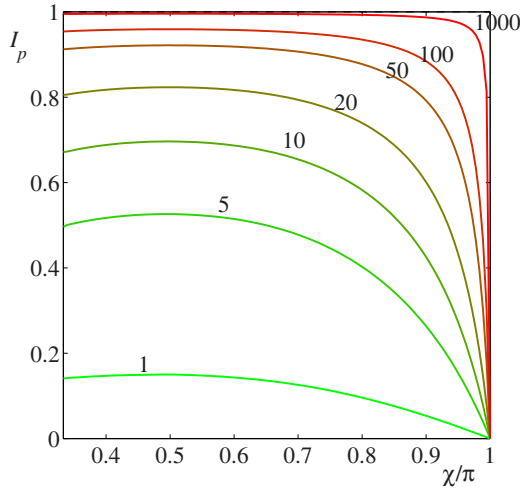

FIG. 7. (Color online) The polarity index I_p at $\alpha=0$ is plotted as a function of $\chi \in [\frac{\pi}{3},\pi]$ for n ranging between 1 and 1000. Upon increasing n, I_p saturates to 1, apart for $\chi=\pi$, where it vanishes, as it should, since there the shapes Ω and Ω' in Fig. 4 lose their polarity.

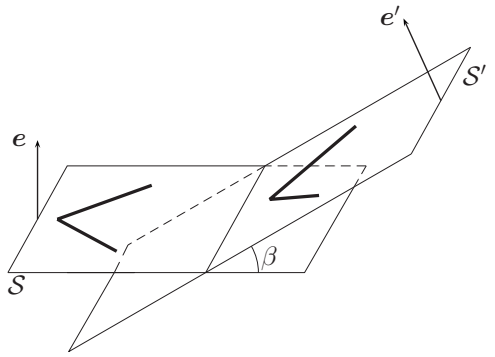

FIG. 8. The symmetry planes $\mathcal{S}$ and $\mathcal{S}'$ are in the "bend" configuration; $\boldsymbol{e}$ and $\boldsymbol{e}'$ are unit vectors orthogonal to $\mathcal{S}$ and $\mathcal{S}'$; $\boldsymbol{e}\cdot\boldsymbol{e}'=\cos\beta=\boldsymbol{p}\cdot\boldsymbol{p}'$. Polar shapes Ω and Ω', outlined as V's, are as in Fig. 4.

this basically results in a two-dimensional effect in their steric interaction. Is it possible to imagine polar shapes that would keep in three space dimensions the same large I_p as in two space dimensions? A natural answer is the shape engendered by revolving a V about its axis $\boldsymbol{p}$, that is, a shape with $C_{\infty v}$ symmetry. For these hollow cones, for example, I_p is a function of the angular amplitude χ and the interaxis angle α which attains its maximum $\frac{3}{5}$ for $\alpha=0$, whatever may be χ. As shown in [9], this maximum is the same as the one for triangles in two space dimensions. For particles with such a polar shape, the antiparallel configuration still minimizes the excluded volume; I_p is smaller than for V-shaped particles, but it persists in the whole solid angle.

We now outline some possible physical consequences of this polar interaction. The most natural of these can be seen in orientationally ordered phases. Nematic phases are induced by either rodlike molecules (calamitic) or flat, disklike molecules (discotic). We first consider calamitic phases constituted by V-shaped molecules. Because of the rapid decay of I_p in both the bend and twist configurations as the angles β and γ grow away from zero, it seems hopeless to produce directly from the isotropic phase any polar order for elongated molecules; possibly, only a nematic uniaxial phase can eventually arise. In such an ordered phase, a polarity effect could appear upon further increasing the density. Our analysis, however, shows that the antiparallel configuration of two V-shaped particles would be favored, and so a uniform polar

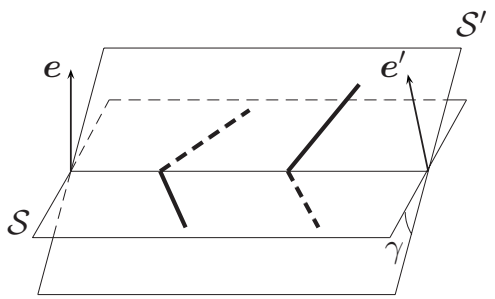

FIG. 9. The symmetry planes $\mathcal{S}$ and $\mathcal{S}'$ are in the "twist" configuration; $\boldsymbol{e}$ and $\boldsymbol{e}'$ are unit vectors orthogonal to $\mathcal{S}$ and $\mathcal{S}'$; $\boldsymbol{e}\cdot\boldsymbol{e}'=\cos\gamma$ and $\boldsymbol{p}\cdot\boldsymbol{p}'=1$. Polar shapes Ω and Ω', outlined as V's, are as in Fig. 4.

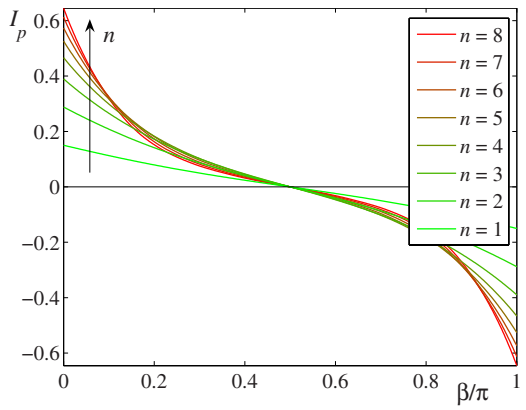

FIG. 10. (Color online) The graph of I_p against the bend angle $\beta \in [0, \pi]$ for polar shapes Ω and Ω' like those in Fig. 4 with $\chi = \frac{\pi}{2}$ and $n = 1, \ldots, 8$, in the configuration illustrated in Fig. 8; an arrow indicates the direction of increase of n through the plots.

order cannot be established, but instead the local antiparallel arrangement of pairs would be statistically equivalent to a single biaxial particle with no polarity. A mixture of parallel and antiparallel V-shaped particles is statistically equivalent to a biaxial platelet, thus justifying the platelet approximation used in [8] to describe the onset of nematic biaxial phases. In general, the ordering of such steric-bound pairs could help enhancing the biaxial phase at large enough density [3–5,12]. To find a significant manifestation of the polar interaction, we must assume a nearly two-dimensional ordering, as for example in well-ordered nematic biaxial phases. Moreover, we see from the sketches in Fig. 1, that in the antiparallel configuration of two V-shaped particles the excluded area starts building up when, in the particles' gliding, the end of one particle comes into contact with the apex of the other. Conversely, in the parallel configuration, the excluded area starts building up when the ends of the gliding particles come mutually in contact. This suggests that by increasing the density in a nearly two-dimensional biaxial phase, so as to confine the particles' wandering in space, an *antiferromorphic* smectic phase could be induced (see Fig. 12). Such a phase, which is also termed either CP_A [13,14] or

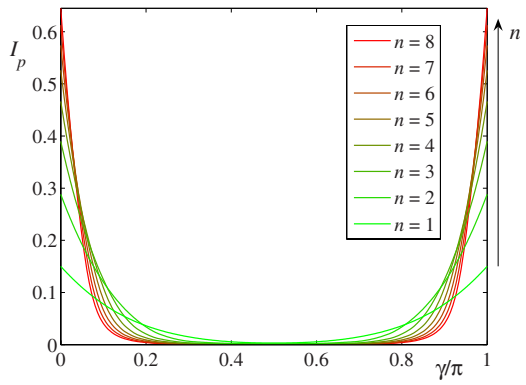

FIG. 11. (Color online) The graph of I_p against the twist angle $\gamma \in [0, \pi]$ for polar shapes Ω and Ω' like those in Fig. 4 with $\chi = \frac{\pi}{2}$ and $n = 1, \ldots, 8$, in the configuration illustrated in Fig. 9; an arrow indicates the direction of increase of n through the plots.

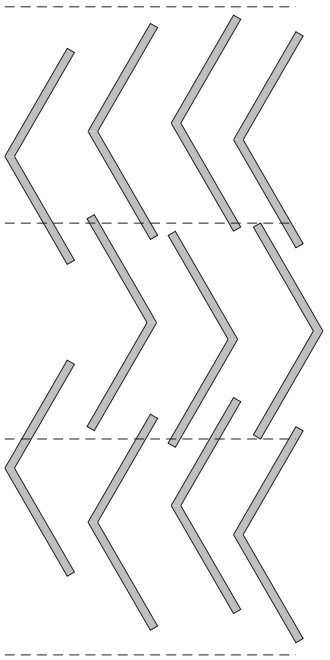

FIG. 12. Antiferromorphic arrangement in a nearly two-dimensional situation. If mutual gliding is hampered by spatial ordering, the shapes Ω and Ω' reduce their excluded area when they are in the parallel configuration within one and the same layer, and in the antiparallel configuration in every pair of adjacent layers.

$SmAP_A$ [15], has already been observed both experimentally [16] and in computer simulations [15,17].

Consider now nematic phases induced by V-shaped molecules interacting via standard dispersion forces. Such molecules can possess a permanent electric dipole, which, by symmetry, must be along $\boldsymbol{p}$. Were we allowed to neglect any steric interaction between two such molecules, the purely electric interaction between them would induce the configuration where the electric dipoles are head-to-tail, and correspondingly the molecules match one on top of the other. However, as shown, for example, in [18] for induced dipole-dipole interactions, steric effects cannot be neglected whenever the molecular electric dipoles, either spontaneous or induced, are well confined within the molecular shape, as is also the case here. For elongated molecules with a permanent electric dipole transverse to the axis of their major extension, it can be shown with the same techniques developed in [18] that the effective pair potential binding two such molecules, supposed to be isotropically distributed in space, is such that their electric dipoles would lie one parallel to the other, for nearly quadrupolar molecular shapes [9], as if they were point dipoles in space not hampered by any steric obstruction [21]. Thus, in a nematic ordering, where these molecules are not organized in space, the parallel dipole ordering is expected to dominate on average. On the other hand, as shown above, the antiparallel configuration favored by the polar excluded volume effect is antagonistic to the parallel configuration favored by the electric dipole-dipole interaction. This competition could explain the small effect on the nematic transition temperature of an added transverse dipole [19]. On the contrary, in the presence of a smecticlike positional or-

dering, the electric dipolar interaction is stronger and it is expected to stabilize the antiferromorphic phase induced by the shape polarity, a phase which is also antiferroelectric.

For discotic phases, the wider angular dependence of I_p is more favorable than for calamitic phases to the appearance at high density of a uniaxial state. Again, molecules could be statistically combined in steric-bound pairs, and so become the building blocks of the uniaxial order. At large densities, we cannot expect polar discotics to build an antiferromorphic discotic columnar phase, because the best columnar hexagonal packing implies frustration for side interactions. In practice, for chemical reasons, most discotic molecules have a flat rigid core with high polarizability and disordered tails distributed around the plane of symmetry. Thus, unfortunately, there is yet no molecule candidate to exhibit the local antiparallel steric binding that we suggest.

Our model is so general as to also apply to nanoparticles and, more interestingly, when their shape is polar and does not belong to any crystallographic class. This would be the case, for instance, for proteins, the packing of which would be dominated by steric interactions. It could be interesting to look for a possible steric pair binding of protein aggregates both in bulk and on membranes.

Similarly, chiral shapes, which we have not discussed so far, are polar. Excluded volume interactions of two chiral enantiomorphic shapes could also produce a steric binding. We are presently studying chiral shapes using the sphere-decomposition technique of [11]. We attempt to establish a possible steric source for the observed large stability of the nematic eutectic produced when mixing in equal proportions two enantiomorphic cholesterics [20].

A word of caution should be said about our speculations above. Our model for steric interactions is entirely based on second-virial arguments, which in principle become less and less stringent as the particles' density is increased. Thus, strictly speaking, knowing that a liquid crystal phase is possible at large densities does not imply that it will indeed be realized: it could still be pre-empted by the appearance of other, more ordered phases. Our speculations outline a number of possible scenarios that need be confirmed by specific predictive means, such as computer simulations.

To conclude, we discussed the effect of excluded volume polarity on the hard-core interaction of polar particles with both biaxial and uniaxial symmetries. We found a counterintuitive tendency to antiparallel ordering opposed to the one that would be favored by electrostatic interactions. For polar, extremely elongated biaxial particles, such a polarity effect is essentially two dimensional and it should be visible in biaxial nematics. For polar uniaxial particles, this effect is three dimensional. For both types of particles, the steric antiparallel binding of two particles could be the building block for the appearance of an effective biaxial or uniaxial order, respectively. Our conclusions also explain the antiferromorphic arrangement observed experimentally and in computer simulations. More generally, we think we indicated an avenue to improve the models that describe steric interactions between polar-shaped particles.

APPENDIX: EXCLUDED AREA COMPUTATIONS

We collect in this appendix the main technical steps needed to compute the excluded area of a pair of V-shaped rods. Let ℓ be the length of both arms in each rod and let $\chi \in [0,\pi]$ be the interarm angle. For definiteness and to reduce the amount of case distinction, we take $\chi \in [\frac{\pi}{2},\pi]$. We denote by $\boldsymbol{m}_1$ and $\boldsymbol{m}_2$ the unit vectors emanating along the arms of one V-shaped rod from its apex P_0 and by $\boldsymbol{m}'_1$ and $\boldsymbol{m}'_2$ the corresponding unit vectors emanating along the arms of the other V-shaped rod from its apex P'_0. For brevity, we shall refer to these shapes as Ω and Ω', respectively.

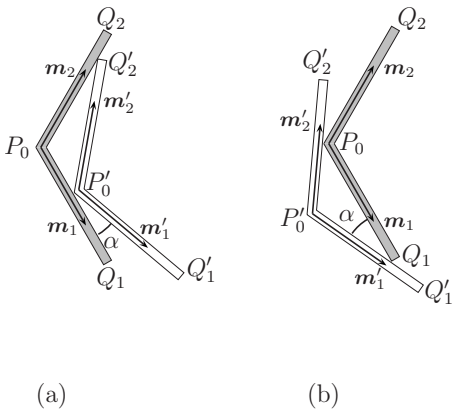

FIG. 13. Configurations with double contact between the V-shaped rods Ω (gray) and Ω' (white). The angle α by which Ω' is rotated relative to Ω is bound to the interval $[0,\pi-\chi]$.

Suppose that the angle α that $\boldsymbol{m}'_1$ makes with $\boldsymbol{m}_1$, the same as the angle that $\boldsymbol{m}'_2$ makes with $\boldsymbol{m}_2$, is in the interval $[0,\pi-\chi]$. Figure 13 illustrates the two typical situations that require some extra care, where the contact between Ω and Ω' takes place in two points. In particular, we can envisage the configuration in Fig. 13(a) as the one from which Ω' starts gliding over Ω. Simple geometric considerations show that

$$a := |P_0 - Q'_2| = \ell \frac{\sin(\alpha+\chi)}{\sin\chi}, \quad b := |P_0 - P'_0| = \ell \frac{\sin\alpha}{\sin\chi}.$$

Figure 13(b) illustrates the other typical configuration with double contact traversed by Ω' in its gliding over Ω. Also in this configuration,

$$|P'_0 - P_0| = b \quad \text{and} \quad |P'_0 - Q_1| = a.$$

It is now a simple matter to see that in the gliding of Ω' over Ω the apex of Ω' describes a simple closed polygonal with the following vertices:

$$P'_0, \quad P'_1 = P'_0 + (\ell - a)\boldsymbol{m}_2, \quad P'_2 = P'_1 + \ell \boldsymbol{m}'_2,$$

$$P'_3 = P'_2 - \ell \boldsymbol{m}'_1, \quad P'_4 = P'_3 - \ell \boldsymbol{m}_2, \quad P'_5 = P'_4 + \ell \boldsymbol{m}_1,$$

$$P'_6 = P'_5 + (\ell - a)\boldsymbol{m}'_1, \quad P'_7 = P'_6 - (\ell - b)\boldsymbol{m}'_2,$$

$$P'_8 = P'_7 + \ell \boldsymbol{m}_1, \quad P'_9 = P'_8 + \ell \boldsymbol{m}'_2$$

$$P'_{10} = P'_9 - (\ell - b)\boldsymbol{m}_1 = P'_0, \tag{A1}$$

where P'_0 is the apex of Ω' in the configuration shown in Fig. 13(a). The excluded area A^* of Ω and Ω' is the area of the polygon with the vertices in (A1).

Choosing any point O within a simple polygon with vertices $\{P'_i,\ i=0,\ldots,N+1\}$, with

$$P'_{N+1} = P'_0, \tag{A2}$$

we can decompose it in the union of $N+1$ triangles with one vertex in O and bases coincident with the sides of the polygon. Thus, the area A^* of such a polygon can be written as

$$A^* = \frac{1}{2}\left|\sum_{i=1}^{N+1}(P'_i - O)\times(P'_{i-1} - O)\right|, \tag{A3}$$

provided that the vertices $\{P'_i\}$ are ordered along one of the two possible orientations of the perimeter of the polygon. It is easily seen that Eq. (A3) is invariant under translation of O, and so this point can be chosen coincident with P'_0. Thus, Eq. (A3) becomes

$$A^* = \frac{1}{2}\left|\sum_{i=1}^{N-1}(P'_{i+1} - P'_i)\times(P'_i - P'_0)\right|, \tag{A4}$$

where use has also been made of (A2).

By applying Eq. (A4) to the chain of vertices in (A1), we arrive at the following expression for $A^*(\alpha)$, valid for $\alpha \in [0, \pi-\chi]$:

$$A^*(\alpha) = \frac{\ell^2}{\sin\chi}[2\sin\chi(\sin\alpha + \cos\alpha\sin\chi) - \sin\alpha\sin(\alpha+\chi)]. \tag{A5}$$

It is much easier to compute A^* in the intervals $[\pi-\chi,\chi]$ and $[\chi,\pi]$, as the contact between Ω and Ω' takes place at a single point for the whole gliding. For completeness, we record here the corresponding sequences of moves:

$$P'_0,\quad P'_1 = P'_0 + \ell\boldsymbol{m}_2,\quad P'_2 = P'_1 + \ell\boldsymbol{m}'_2,$$
$$P'_3 = P'_2 - \ell\boldsymbol{m}'_1,\quad P'_4 = P'_3 - \ell\boldsymbol{m}_2,\quad P'_5 = P'_4 + \ell\boldsymbol{m}_1,$$
$$P'_6 = P'_5 + \ell\boldsymbol{m}'_1,\quad P'_7 = P'_6 - \ell\boldsymbol{m}'_2,$$
$$P'_8 = P'_7 - \ell\boldsymbol{m}_1 = P'_0, \tag{A6}$$

and

$$P'_0,\quad P'_1 = P'_0 + \ell\boldsymbol{m}_2,\quad P'_2 = P'_1 + \ell\boldsymbol{m}'_2,$$
$$P'_3 = P'_2 - \ell\boldsymbol{m}_2,\quad P'_4 = P'_3 - \ell\boldsymbol{m}'_1,\quad P'_5 = P'_4 + \ell\boldsymbol{m}_1,$$
$$P'_6 = P'_5 + \ell\boldsymbol{m}'_1,\quad P'_7 = P'_6 - \ell\boldsymbol{m}'_2,$$
$$P'_8 = P'_7 - \ell\boldsymbol{m}_1 = P'_0. \tag{A7}$$

Correspondingly, the formulae for A^* read as follows:

$$A^*(\alpha) = 2\ell^2\sin\alpha(1-\cos\chi),\quad \alpha\in[\pi-\chi,\chi] \tag{A8}$$

and

$$A^*(\alpha) = \ell^2[2\sin\alpha - \sin(\alpha+\chi)],\quad \alpha\in[\chi,\pi]. \tag{A9}$$

Equations (A5), (A8), and (A9) have been employed in Sec. II to describe the polarity exhibited by the purely steric interaction of two V-shaped rods in two space dimensions, the specific example at the start of our study.

[1] L. Onsager, Ann. N.Y. Acad. Sci. **51**, 627 (1949). Reprinted in T. J. Sluckin, D. A. Dunmur, and H. Stegemeyer, *Crystals that Flow* (Taylor and Francis, London, New York, 2004), pp. 625–657.

[2] T. Hegmann, H. Qi, and V. M. Marx, J. Inorg. Organomet. Polym. **17**, 483 (2007).

[3] L. A. Madsen, T. J. Dingemans, M. Nakata, and E. T. Samulski, Phys. Rev. Lett. **92**, 145505 (2004).

[4] B. R. Acharya, A. Primak, and S. Kumar, Phys. Rev. Lett. **92**, 145506 (2004).

[5] K. Severing and K. Saalwächter, Phys. Rev. Lett. **92**, 125501 (2004).

[6] G. R. Luckhurst, Nature (London) **430**, 413 (2004).

[7] K. Severing, E. Stibal-Fischer, A. Hasenhindl, H. Finkelmann, and K. Saalwächter, J. Phys. Chem. B **110**, 15680 (2006).

[8] P. I. C. Teixeira, A. J. Masters, and B. M. Mulder, Mol. Cryst. Liq. Cryst. Sci. Technol., Sect. A **323**, 167 (1998).

[9] G. E. Durand and E. G. Virga (unpublished).

[10] See, for example, G. S. Singh and B. Kumar, Ann. Phys. (N.Y.) **294**, 24 (2001).

[11] F. Bisi and R. Rosso (unpublished).

[12] G. R. Luckhurst, Angew. Chem., Int. Ed. **44**, 2834 (2005).

[13] H. R. Brand, P. E. Cladis, and H. Pleiner, Macromolecules **25**, 7223 (1992).

[14] H. R. Brand, P. E. Cladis, and H. Pleiner, Eur. Phys. J. B **6**, 347 (1998).

[15] Y. Lansac, P. K. Maiti, N. A. Clark, and M. A. Glaser, Phys. Rev. E **67**, 011703 (2003).

[16] A. Eremin, S. Diele, G. Pelzl, H. Nádasi, W. Weissflog, J. Salfetnikova, and H. Kresse, Phys. Rev. E **64**, 051707 (2001).

[17] R. Memmer, Liq. Cryst. **29**, 483 (2002).

[18] A. M. Sonnet and E. G. Virga, Phys. Rev. E **77**, 031704 (2008).

[19] S. Chandrasekhar, *Liquid Crystals*, 2nd ed. (Cambridge University Press, Cambridge, 1992). See, in particular, Sect. 2.6.2.

[20] A. M. Levelut, C. Germain, P. Keller, L. Liebert, and J. Billard, J. Phys. (Paris) **44**, 623 (1983).

[21] It can also be shown [9] that, conversely, when the permanent electric dipole is parallel to the major molecular axis, the effective pair potential would induce the configuration in which the dipoles are antiparallel.